Modeling of Liquid Water Distribution at Cathode Gas Flow Channels in Proton Exchange Membrane Fuel Cell - PEMFC

Sandro Skoda[1*], Eric Robalinho[2], André L. R. Paulino[1], Edgar F. Cunha[1], Marcelo Linardi[1]

[1]Instituto de Pesquisas Energéticas e Nucleares IPEN
[2]Universidade Nove de Julho UNINOVE

*Av. Prof. Lineu Prestes, 2242, Cidade Universitária, 05508-000, São Paulo-SP, Brazil,
e-mail: sandroskoda@gmail.com

Abstract: The objective of this study is to determine the locations where liquid water accumulates at cathode gas flow channels, and the corresponding operating conditions. In such way it is possible to mitigate slug flow, responsible for channel blockage and hindering the diffusion of reactants to the catalytic sites. The electrochemical reactions responsible by the performance of PEM fuel cell can be optimized by controlling the operating conditions. The model presented here is a comprehensive PEMFC 3D model, which includes liquid water phase detection along the flow direction, and transport of gaseous species, protons and energy. Computational models of fuel cells have been an important optimization tool to fuel cell development. The experimental data from a transparent-cathode-channels-fuel cell set up were used to validate the computational model. The investigated parameters were: temperature (298 – 358K); flow rates (H_2: 200 - 300 ml/min and O_2: 100 - 150 ml/min); and potential (0.1 - 1.0 V). The software for modeling was COMSOL Multiphysics 4.3a.

Keywords: Fuel cell, modeling, water distribution, slug-flow, flooding.

1. Introduction

Fuel cells are electrochemical systems that transform the chemical energy of a fuel directly into electricity and heat, possessing, however, a continuous operation, thanks to the power contained in a fuel [1]. Its properties are remarkable high efficiency in energy conversion and zero emissions that meet the energy needs of a rapidly growing society. Among all types of fuel cell, the Proton Exchange Membrane Fuel Cell (PEMFC), also called a Polymer Electrolyte Fuel Cell (PEFC) reached an early stage of development particularly for portable and automotive applications. In addition to its high power density, the PEM fuel cells working at low temperatures producing only water as a byproduct and can be mounted compactly. A PEMFC is typical of bipolar plates, gas channels, gas diffusion layers (GDLs) and a proton conductive membrane with catalytic layer (platinum catalyzed) on each side, called a Membrane Electrode Assembly (MEA) and shown in Figure 1.

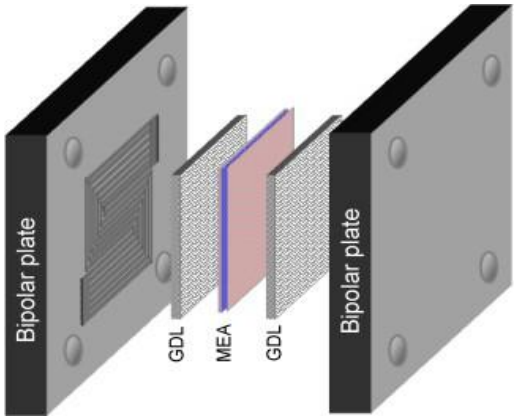

Figure 1. Schematic of a PEM fuel cell. [2]

The gas channels are machined in bipolar plates through which the reagents and are distributed to the electrochemical reactions.

The GDLs play an important role in electronic connection between the bipolar plate and the electrodes and provide a passage for the transport of reactants and removal of heat and water. The protons are produced by the oxidation of hydrogen in the anode catalytic layer and pass through the membrane, carrying water molecules via electro osmotic drag to the cathode catalytic layer occurs where the oxygen reduction reaction (ORR) with water as a byproduct.

The operation of PEM fuel cells occurs from the continuous external supply of a fuel, usually

hydrogen. At the anode, the oxidation of H_2 generates protons and electrons. The electrons are transported through an external circuit from the anode to the cathode, while the protons are transported to the cathode through the electrolyte. The reaction of O_2 reduction occurs at the cathode, where protons (from the anode) plus electrons (from the external circuit) combine to form water and heat.

The electrochemical reactions that take place simultaneously at both sides of membrane are the following:

At the anode:

$$H_2 \rightarrow 2H^+ + 2e \quad (1)$$

At the cathode:

$$\tfrac{1}{2}O_2 + 2H^+ + 2e^- \rightarrow H_2O \quad (2)$$

Overall:

$$H_2 + \tfrac{1}{2}O_2 \rightarrow H_2O \quad (3)$$

The water management is a key technology in PEM fuel cells because while water is essential for the ionic conductivity in the membrane, excess water leads to flooding liquid of the GDLs and catalyst layers (CLs) as well as the blocking of channels.

Given the low operating temperatures during normal start (298K) and therefore low saturation pressures, two-phase phenomena are inevitable in automotive fuel cells.

The water transport in a fuel cell presents some types of problems such as catalytic layer flooding, GDL flooding and two-phase flow in channels. In the literature, there are few models dealing with the flooding in channels.

In practice, the water transport is extremely important to the operation of PEM fuel cell system particularly at high-potential and therefore low current density. In this operation regime the flow rates of hydrogen and oxygen through the channels are low resulting in a substantial accumulation of liquid water.

Other important considerations about flooding the channel include: stagnation of the gas that leads to corrosion of the carbon in the cathode catalyst layer, leading the formation of hot spots; misdistribution of flow between parallel channels leading to instability and loss of operating efficiency; increased mass transport losses in high current densities.

There is therefore a pressing need in terms of developing a model for water transport analysis, particularly in flow channel PEM fuel cells for the prediction of high levels of saturation of liquid water.

2. Governing Equations

The numerical model used conservation equations, reaction equations and constitutive relations, such as:

- Tafel equation for the reaction in the cathode catalyst layer;
- Butler-Volmer equation for the reaction in the anodic catalyst layer;
- Ohm's law for the ionic and electronic charge transport;
- Navier-Stokes equations for the free flow in the channels;
- Brinkman equations for the flow in porous layers;
- Maxwell-Stefan equations for chemical species transport in the gas phase;
- Mass transfer rate from liquid to vapor for anode and cathode catalyst layers, GDLs and gas channels.[3]

Assumptions used in this model are:

- ideal gas properties;
- ideal gas mixtures;
- compressible flow;
- laminar flow;
- isotropic and homogeneous membrane and electrode structures;
- steady state.

The electrochemical reactions described by Equations (1) - (3) take place in the electrodes, and their kinetics, responsible for activation overpotential, is described by the Butler-Volmer equation:

$$i = i_0 \left[\exp\left(\frac{-\alpha_R F}{RT}\eta\right) - \exp\left(\frac{\alpha_O F}{RT}\eta\right) \right] \quad (4)$$

where i is the current density, i_0 is the exchange current density, α_R and α_O are the transfer coefficients, T is the operating temperature, F and R are the Faraday and the gas constants and η is the overpotential.

When the overpotential is high as the case for the cathode, the Butler-Volmer equation is simplified to the Tafel equation:

$$\eta = A\ln\left(\frac{i}{i_0}\right) \quad (5)$$

where A is Tafel slope.

Charge transport in the electrode and electrolyte is based on Ohm's law, namely:

$$\nabla \boldsymbol{i_k} = \boldsymbol{Q_k} \quad (6)$$

$$\boldsymbol{i}_k = -\sigma_k \nabla \phi_k \quad (7)$$

where $\boldsymbol{i}_k$ is the current density, $\boldsymbol{Q}_k$ is a source term, σ_k is the conductivity and ϕ_k is the potential, while k denotes an index that is l for the electrolyte and s for the electrode.

In the channels, gas flow is governed by the Navier-Stokes equations for compressible fluids:

$$\nabla.(\rho \boldsymbol{u}) = 0 \quad (8)$$

$$\rho \boldsymbol{u}.\nabla \boldsymbol{u} = -\nabla.(-p\boldsymbol{I} + \tau) \quad (9)$$

$$\tau = \mu[\nabla \boldsymbol{u} + (\nabla \boldsymbol{u})^T] - \frac{2}{3}\mu(\nabla.\boldsymbol{u})\boldsymbol{I} \quad (10)$$

where ρ is the density, $\boldsymbol{u}$ is the velocity vector, p is the pressure, τ is the viscous stress tensor and μ is the dynamic viscosity.

In porous media, found in the catalyst and diffusion layers, the Navier-Stokes is changed into the Brinkman equations:

$$\nabla.(\rho \boldsymbol{u}) = \boldsymbol{Q}_{br} \quad (11)$$

$$\frac{\rho}{\varepsilon_p}\left[(\boldsymbol{u}.\nabla)\frac{\boldsymbol{u}}{\varepsilon_p}\right] = \nabla.\left(-p\boldsymbol{I} + \frac{\tau}{\varepsilon_p}\right) - \left(\frac{\mu}{K} + \frac{\boldsymbol{Q}_{br}}{\varepsilon_p^2}\right)\boldsymbol{u} \quad (12)$$

where $\boldsymbol{Q}_{br}$ is a mass source or sink, ε_p is the porosity and K is permeability of the porous media.

Chemical species transport in ideal gas mixtures is described by the Maxwell-Stefan equation:

$$\rho(\boldsymbol{u}.\nabla)\omega_i = \nabla.\left(\rho\omega_i \sum_{k=1}^{Q} \widetilde{\boldsymbol{D}}_{ik}\, d_k\right) + R_i \quad (13)$$

$$\boldsymbol{d}_k = \nabla x_k + \frac{1}{p}[(x_k - \omega_k)\nabla p] \quad (14)$$

$$x_k = \frac{\omega_k}{M_k}\bar{M} \quad (15)$$

$$\frac{1}{\bar{M}} = \sum_{i=1}^{Q}\frac{\omega_i}{M_i} \quad (16)$$

where the indexes i and k represent different species, ρ is the mixture density, ω_i is the mass fraction, $\widetilde{\boldsymbol{D}}_{ik}$ are the multicomponent diffusivities, $\boldsymbol{d}_k$ is the diffusional driving force, R_i is the rate of production or consumption, x_k is the mole fraction, p is the total pressure, M_k is the molar mass and $\bar{M}$ is the mean molar mass of the mixture.

Mass transfer among the phases and equilibrium constraints are implemented by the source term of Eq. (17) and switch function given by Eq. (18). The equilibrium between liquid and vapor phases is maintained by Eq. (17) which a large positive value for the term S_{LV} (corresponding to rapid evaporation) if liquid is present and the adjacent vapor exists at a pressure below saturation. Conversely if the pressure of the vapor phase exceeds the saturation pressure, the term S_{LV} exhibits a large negative value (corresponding to rapid condensation).

$$S_{LV} = \psi s \gamma_{LV} - \psi(1-s)(1-\gamma_{LV}) \quad (17)$$

where s is the saturation, ψ is the evaporation/condensation mass transfer coefficient and γ_{LV} is the switch function. Equilibrium control function liquid/vapor switch,

γ_{LV} is one for $\frac{\rho_{WV}^g}{\rho_{SAT}^g} < 0.98$, else zero.

$$\gamma_{LV} = 1 - 0.5\left[1 + \tanh\left(61\frac{\rho_{WV}^g}{\rho_{SAT}^g} - 59\right)\right] \quad (18)$$

where ρ_{WV}^g is the density of water vapor in the gas phase and ρ_{SAT}^g is the density of saturated vapor in the gas phase.

3. Numerical Model

The 3D model used in this study, as shown in Figure 2, a fuel cell with 5 cm² active area, is similar to experimental transparent fuel cell used

in this work. The plates have 9 parallel flow channels with width of 1.0 mm, depth of 1.0 mm and length of 23.2 mm, intercalated with 1.8 mm ribs. The meshes constructed (Figure 3) are completely structured composed exclusively of hexahedral elements. The mesh consist of 506k elements for the parallel channels model.

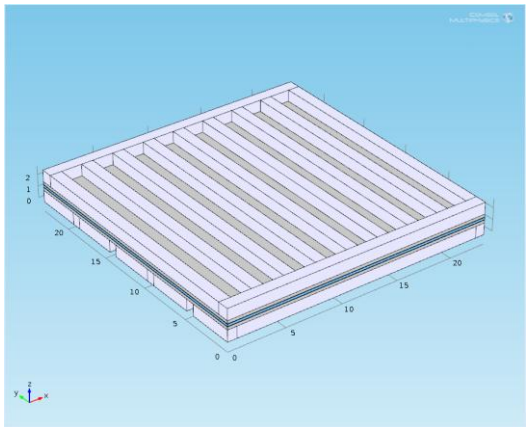

Figure 2. Geometry used in the parallel channels model.

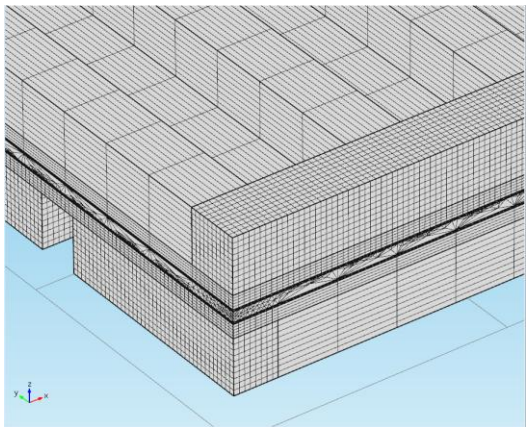

Figure 3. Mesh detail for the parallel channels model.

As a simplification, the system is isothermal and all chemical species are considered ideal gases. The cell operates in steady-state, the flow is laminar (low Reynolds number) and all materials properties are homogeneous.

Electrochemical reactions and charge transport were modeled using the Secondary Current Distribution interface. Free and Porous Media Flow interface was used for modeling momentum transport. Diffusion of reactants and products was modeled with the Transport of Concentrated Species interface.

4. Experimental set up

The experimental set up shown in Figure 4 consists of: i) a fuel and oxidant reactant supply system; ii) a cell performances test system; iii) a digital camera recording system; iv) a data collector and analysis system.

The images of water flooding in the cathode flow channels were recorder by a Nikon Coolpix P7000 digital camera.

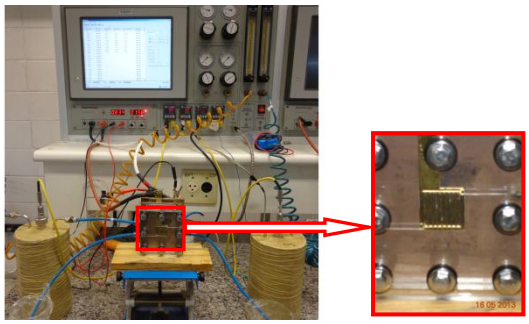

Figure 4. Transparent cathode channels fuel cell set up; inset: channels view.

5. Results

Polarization curves for experimental data and numerical data were plotted and are shown in Figure 5. The plots show that polarization curve for experimental data (blue dots) is a good concordance with polarization curve for numerical data (red line). Therefore, it's implied that parallel flow channels model is validated.

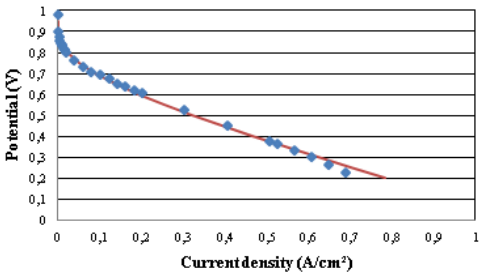

Figure 5. Polarization curves for experimental data (blue dots) and numerical data (red line) at 328 K.

Numerical results for water mole fraction distribution, 328K, 0.6V, are showed in Figure 6. The results for the saturation distribution, at the conditions, are showed in Figure 7.

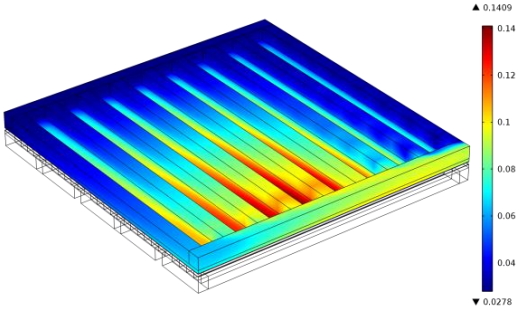

Figure 6. Numerical results: water mole fraction distribution, 328K, 0.6V.

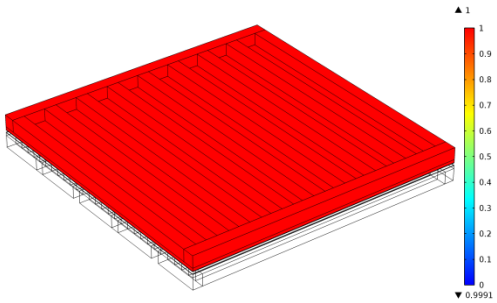

Figure 7. Numerical results: saturation distribution, 328K, 0.6V, blue color represents saturation water (more than 98%), red color represents vapor water (less than 98%).

A new experiment was carried out at the 308K, and the polarization curves are showed in Figure 8, with the correspondents numerical responses showed in Figure 9 and Figure 10.

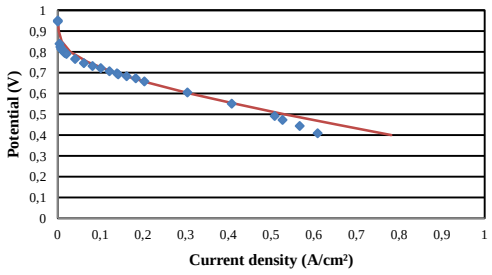

Figure 8. Polarization curves for experimental data (blue dots) and numerical data (red line) at 308K.

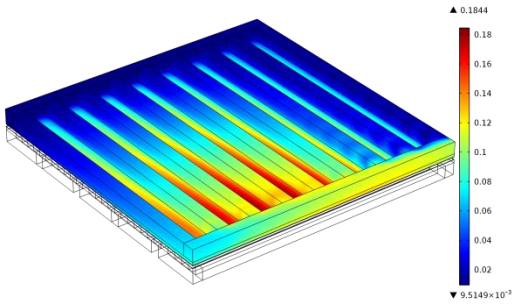

Figure 9. Numerical results: water mole fraction distribution, 308K, 0.6V.

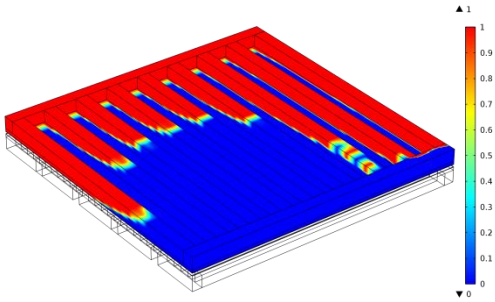

Figure 10. Numerical results: saturation distribution, 308K, 0.6V, blue color represents saturation water (more than 98%), red color represents vapor water (less than 98%).

A sequence of numerical responses, as showed in Figures 11 (a) and (b), contribute to demonstrate the importance of computational simulations in the water management analysis, at different temperatures and potentials of the fuel cell. In the Figure 11 (a) are showed the responses to water saturation level, at 298K, 0.4 V and (b) at 0.6 V.

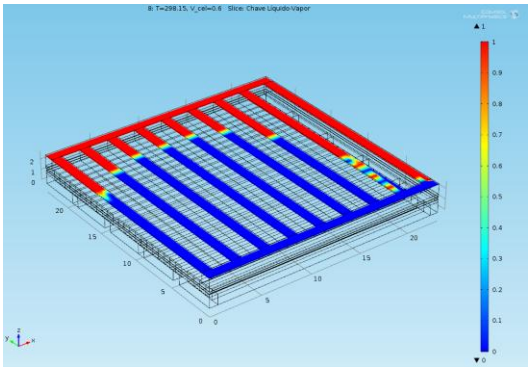

(a)

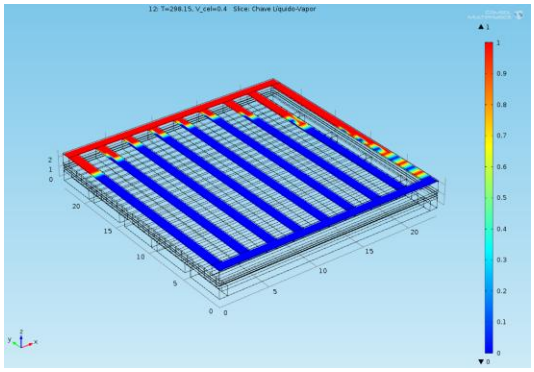

(b)

Figure 11. Numerical results: slice plot of water saturation level: (a) 0.6 V and (b) 0.4 V, blue color represents saturation water (more than 98%), red color represents vapor water (less than 98%).

It was noticed that in Figure 11, the quantity of water saturation increased when the potential decreased. It was showed in details when the cell potential drops, as observed in (a) to (b). It means that the volume of saturation water in the channels of (b) is greater than the correspondent numerical simulation result in a lower potential (a).

In the images showed in Figures 12 (a) and (b) it is possible to notice the formation of water vapor and, progressively, the coalescence of the droplets, resulting finally the water column (slug). The transparent cathode channels fuel cell set up allowed the visualization of that process, and these pictures proved the slug formation.

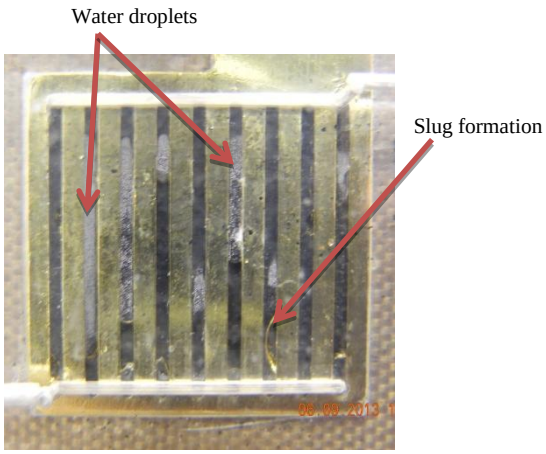

(a)

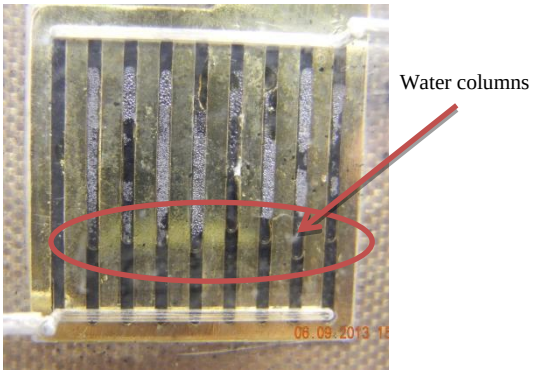

(b)

Figure 12. Experimental results: cathode water droplets build-up in flow channels with time: (a) 5 min; (b) 15 min. Operation conditions: 298K, 0.4 A/cm^2, O_2 non humidified, ambient pressure.

6. Conclusions

The liquid water observed in the flow field decreased with the increase of cell temperature. During the operation of the fuel cell, the oxygen flow rate could contribute to water removal, avoiding the slug formation. Water flooding might occur if the produced water was not removed quickly from the channels. The implementation of the switch function improved the model allowing the visualization of the saturated and vapor water at the channels, as noticed in water saturation level figures.

7. References

1. Marcelo Linardi, Introdução à Ciência e Tecnologia de Células a Combustível, Art Lieber Editora, São Paulo, SP (2010)

2. Y.Wang et al., Modeling two-phase flow in PEM fuel cell channels, Journal of Power Sources, V.179, pp.603-617 (2008).

3. N.P.Siegel et al., A two-dimensional computational model of a PEMFC with liquid water transport, Journal of Power Sources, V.128, pp.173-184 (2004).